https://rbgeomorfologia.org.br/
ISSN 2236-5664

Revista Brasileira de Geomorfologia

v. 24, nº 2 (2023)

http://dx.doi.org/10.20502/rbg.v24i2.2311

Research Article

Morphometric parameters of the relief and drainage network of the Formiga River subbasin, Minas Gerais, Brazil

Parâmetros morfométricos do relevo e da rede de drenagem da sub-bacia hidrográfica do rio Formiga, Minas Gerais, Brasil

Igor Luís Reis [1], Gustavo Sousa Marinho[2], Guilherme da Silva Rios[3], Derielsen Brandão Santana[4], Guilherme Henrique Expedito Lense[5], Ronaldo Luiz Mincato[6], Felipe Gomes Rubira[7]

[1] Universidade Federal de Alfenas (UNIFAL-MG), Alfenas, Brasil. igor.reis@sou.unifal-mg.edu.br
ORCID: https://orcid.org/0000-0002-5876-0083

[2] Universidade Federal de Alfenas (UNIFAL-MG), Alfenas, Brasil. gustavo.marinho@sou.unifal-mg.edu.br
ORCID: https://orcid.org/0000-0003-1393-3822

[3] Universidade Federal de Alfenas (UNIFAL-MG), Programa de Pós-graduação em Ciências Ambientais, Alfenas, Brasil. guilherme.rios@sou.unifal-mg.edu.br
ORCID: https://orcid.org/0000-0003-2141-7617

[4] Universidade Federal de Alfenas (UNIFAL-MG), Programa de Pós-graduação em Ciências Ambientais, Alfenas, Brasil. derielsen.santana@sou.unifal-mg.edu.br
ORCID: https://orcid.org/0000-0003-2484-9984

[5] Universidade Federal de Alfenas (UNIFAL-MG), Programa de Pós-graduação em Ciências Ambientais, Alfenas, Brasil. guilherme.lense@sou.unifal-mg.edu.br
ORCID: https://orcid.org/0000-0002-3560-9241

[6] Universidade Federal de Alfenas (UNIFAL-MG), Instituto de Ciências da Natureza, Alfenas, Brasil. ronaldo.mincato@unifal-mg.edu.br
ORCID: https://orcid.org/0000-0001-8127-0325

[7] Universidade Federal de Alfenas (UNIFAL-MG), Instituto de Ciências da Natureza, Alfenas, Brasil. felipe.rubira@unifal-mg.edu.br
ORCID: https://orcid.org/0000-0002-6594-8228

Received: 20/10/2023; Accepted 28/02/2023; Published: 27/06/2023

Abstract: This research analyzed the morphological/morphometric parameters of the relief and drainage network of the Formiga River subbasin, southern Minas Gerais State, Brazil, aiming at identification and the exam the influences of control mechanisms in the development of current configurations. The methodology was based on the application of indices and parameters: (1) slope length (Hack's Sl); (2) normalized slope index (Ksn); (3) river hierarchy; (4) drainage density; (5) hydrographic density; (6) sinuosity index; (7) density of structural lineaments; (8) transverse topographic symmetry factor; (9) asymmetry factor of drainage basins; (10) topographic profiles transverse to the valleys; (11) relief ratio; (12) roughness index; (13) roughness concentration index; (14) compactness coefficient; (15) circularity index; and (16) form factor. The results indicated three sectors with distinct geomorphic behaviors, which resulted in peculiar surface structures and divergent current dynamics. The Formiga River subbasin presents physical evidence that demonstrates and corroborates with the structural control in the development of the current drainage network and relief. The construction of dams affected the dynamics of the lower course of the river, drowned by the reservoir of the hydroelectric plant of Furnas.

Keywords: Structural control; carving; anthropic changes.

Resumo: Esta pesquisa analisou os parâmetros morfológicos/morfométricos do relevo e da rede de drenagem da sub-bacia do rio Formiga, sul do Estado de Minas Gerais, Brasil, visando a identificação e o exame das influências dos mecanismos de controle no seu desenvolvimento. A metodologia foi pautada na aplicação dos índices e parâmetros: (1) *slope lenght* (Sl de Hack); (2) índice normalizado de declividade (Ksn); (3) hierarquia fluvial; (4) densidade de drenagem; (5) densidade hidrográfica; (6) índice de sinuosidade; (7) densidade de lineamentos estruturais; (8) fator de simetria topográfica transversa; (9) fator de assimetria de bacias de drenagem; (10) perfis topográficos transversais aos vales; (11) relação de relevo; (12) índice de rugosidade; (13) índice de concentração de rugosidade; (14) coeficiente de compacidade; (15) índice de circularidade e (16) fator forma. Os resultados indicaram 3 setores da sub-bacia com comportamentos geomórficos distintos, que acarretaram em estruturas superficiais peculiares e com dinâmicas atuais divergentes. A sub-bacia apresenta evidências físicas que demostram e corroboram com o controle estrutural no desenvolvimento da atual rede de drenagem e do relevo. A construção de barragens afetou a dinâmica do baixo curso do rio, afogado pelo reservatório da usina hidrelétrica de Furnas.

Palavras-chave: Controle estrutural; esculturação; modificações antrópicas.

1. Introduction

Research that uses spatial clippings of hydrographic basins from a systemic perspective is relevant, as in addition to reflecting the conditions of natural systems (structure and functioning), they also offer support to environmental management. The physical–natural elements, such as climate, rock, soil, relief, vegetation, and hydrography, have specific attributes that are modified by the inputs and outputs of matter and energy in the system, imposing the reorganization and modification of the landscape (SOTCHAVA, 1977). In Brazil, studies have aimed to investigate the morphological and morphometric patterns of the relief and drainage network of hydrographic basins (BARROS; REIS, 2019). Such studies have explained the genesis of fluvial surfaces from morphometric indices that assess the influence of tectonic (ETCHEBEHERE, 2004; SOUZA; MARTINS; DE FARIA, 2011; COUTO; FORTES; FERREIRA, 2013; PASSARELA; LADEIRA; LIESENBERG, 2016), hydrological (DOMINGUES et al., 2020; SILVA et al., 2021), structural (LAVARANI; MAGALHÃES JÚNIOR, 2013; MONTEIRO; TAVARES; CORRÊA, 2014; LIMA et al., 2017; ALVES et al., 2022; ALVES; ROSSETTI; VALERIANO, 2020; PANTA; NASCIMENTO; MONTEIRO, 2022; ROSSETTI et al., 2022), and anthropic processes (CALIL et al., 2012; ALMEIDA et al., 2013) on the changes in the morphologies of river channels and subbasins (PAIXÃO; SALGADO; FREITAS, 2019).

The morphology of a river is directly related to the bedrock geology (MONTGOMERY et al., 1996). However, the fluvial erosion and deposition dynamics differ significantly between rivers that run through rocky substrates and those over alluvial beds of siliciclastic sediments (TOONE; RICE; PIÉGAY, 2014). The methods developed by Hack (1973) and Kirby and Whipple (2012) have contributed to identifying drainage anomalies generated by structural, climatic, and anthropic processes, mainly in rivers with mixed beds (rocky and alluvial) and/or with different lithotypes.

In general, rivers with mixed beds alternate longitudinally between (i) deep valleys with steep slopes and sloping fluvial channels generally directly on a rocky substrate, with a predominance of erosion due to the high strength of the gradient (WOHL; MERRITT, 2001; PHILLIPS; LUTZ, 2008; WHIPPLE et al., 2022); and (ii) wide valleys with gently undulating slopes and relatively flat fluvial channels and with a predominance of sediment accommodation zones and meandering alluvial beds due to reduced downstream flow energy (MUELLER; PITLICK, 2013; THAYER; ASHMORE, 2016). These fluvial morphologies can be explained by different factors, among which are the erosive gradient potential changes between upper, middle, and lower courses, depending on the flow energy, sediment load, mean sediment diameter, channel slope, and average discharge (CHORLEY; SCHUMM; SUGDEN, 1985; SCHUMM, 1986). The intensity of these variables defines and alters the patterns of fluvial channels from allogeneic, autogenic, and anthropic modifications (DANIELS, 2008; PERȘOIU et al., 2022). Thus, drainage anomalies are indicators of fluvial dynamics and erosive and depositional readjustments (CASTILLO; BISHOP; JANSEN, 2013).

From this theoretical framework, this research aimed to characterize and analyze morphometric parameters of the relief and drainage network of the hydrographic subbasin of the Formiga River subbasin (Minas Gerais, Brazil) (Figure 1), identifying and considering the influences of its control mechanisms. The analysis proved to be effective in compartmentation the basin, revealing three sectors with different geomorphic behaviors that

corroborate considerable structural control in the development of the drainage network and relief. The integration between the indices was successful in investigating the control mechanisms operating in the Formiga River hydrographic subbasin and can be replicated to other areas.

2. Study Area

The Formiga River subbasin is located in the western mesoregion of the State of Minas Gerais and is part of the Grande River Basin (Figure 1).

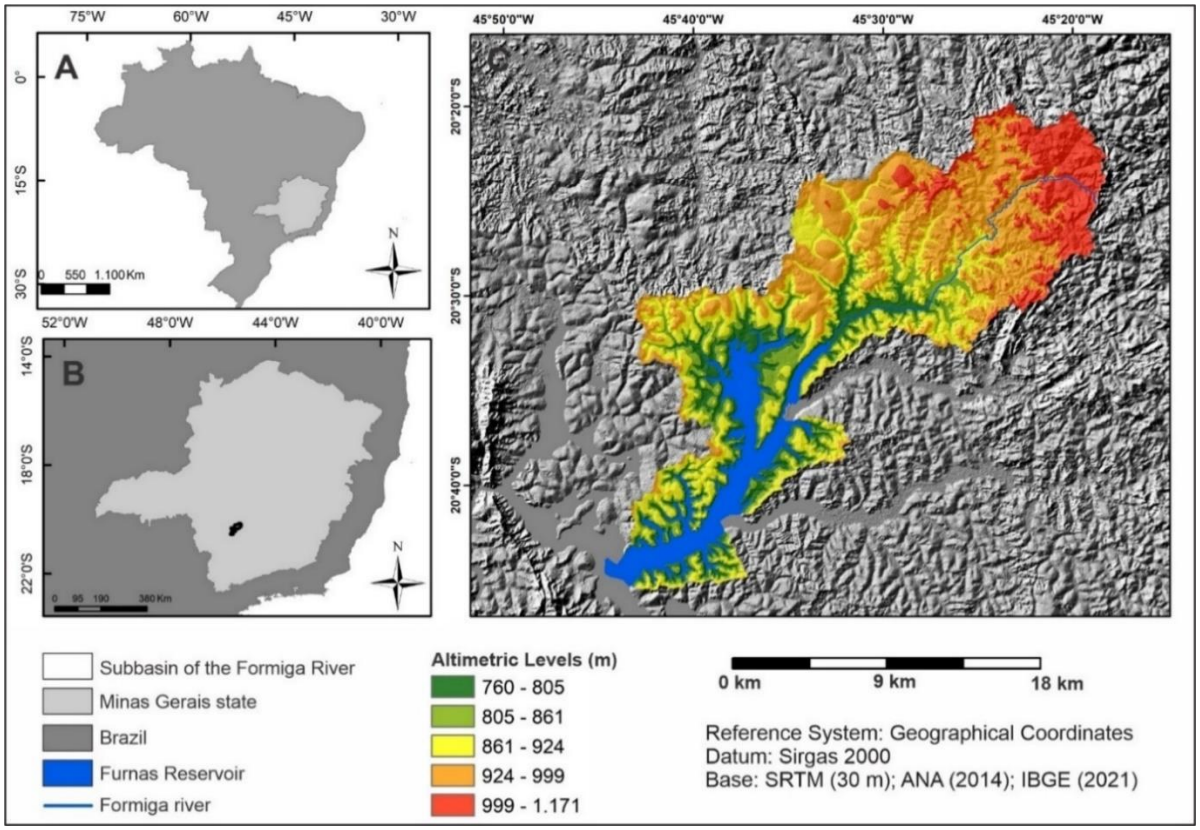

Figure 1. (A) Location of the State of Minas Gerais in Brazil. (B) Location of the Formiga River subbasin in the State of Minas Gerais, Brazil. (C) Hillshade and altimetric map of the Formiga River subbasin based on 30 m digital elevation model from Shuttle Radar Topography Mission (SRTM) (USGS, 2023).

This basin is located over the crystalline basement of the Proterozoic age, which is composed of orthoderived metamorphic rocks and igneous rocks in the upper and middle course of the river. The lower course is dominated by paraderived metamorphic rocks associated with marine transgressions and regressions that covered the São Francisco River Craton. Quaternary clastic sediments cover the alluvial segments (Figure 2A) (SILVA et al., 2020). The main paraderived and orthoderived lithological units and alluvial deposits in the subbasin are shown in Figure 2A.

The drainage network of the Formiga River consists of channels with a dendritic pattern, especially in the upper reaches. The reservoir of the Furnas Hydroelectric Power Plant (UHE) is located in the lower course (Figure 2B). The climate, according to the Köppen classification (1936), is humid subtropical with dry winters and hot summers (Cwb) and humid subtropical with dry winters and temperate summers (Cwa) (ALVARES et al., 2014).

The biomes correspond to the Atlantic Forest and Cerrado (savanna). As this area is a transition zone between the two biomes, the vegetation has different physiognomies, with small trees, undergrowth, and forest vegetation (RIBEIRO; WALTER, 1998). In the Formiga River subbasin, the Atlantic Forest occurs predominantly at higher altitudes and has a Cwb climate, while the Cerrado (savanna) occurs at lower altitudes, and has a Cwa climate.

The relief is characterized by hills and floodplains distributed between 1170 and 753 m in altitude. Hills are located upstream at higher altitudes and slopes. Downstream, there are lower-elevation hills, floodplains, and

gentler slopes. A rolling relief is dominant (50.02%), followed by slightly rolling relief (24.88%), flat (13.92%), strongly rolling relief (10.02%), mountainous (1.13%), and steep relief (0.03%).

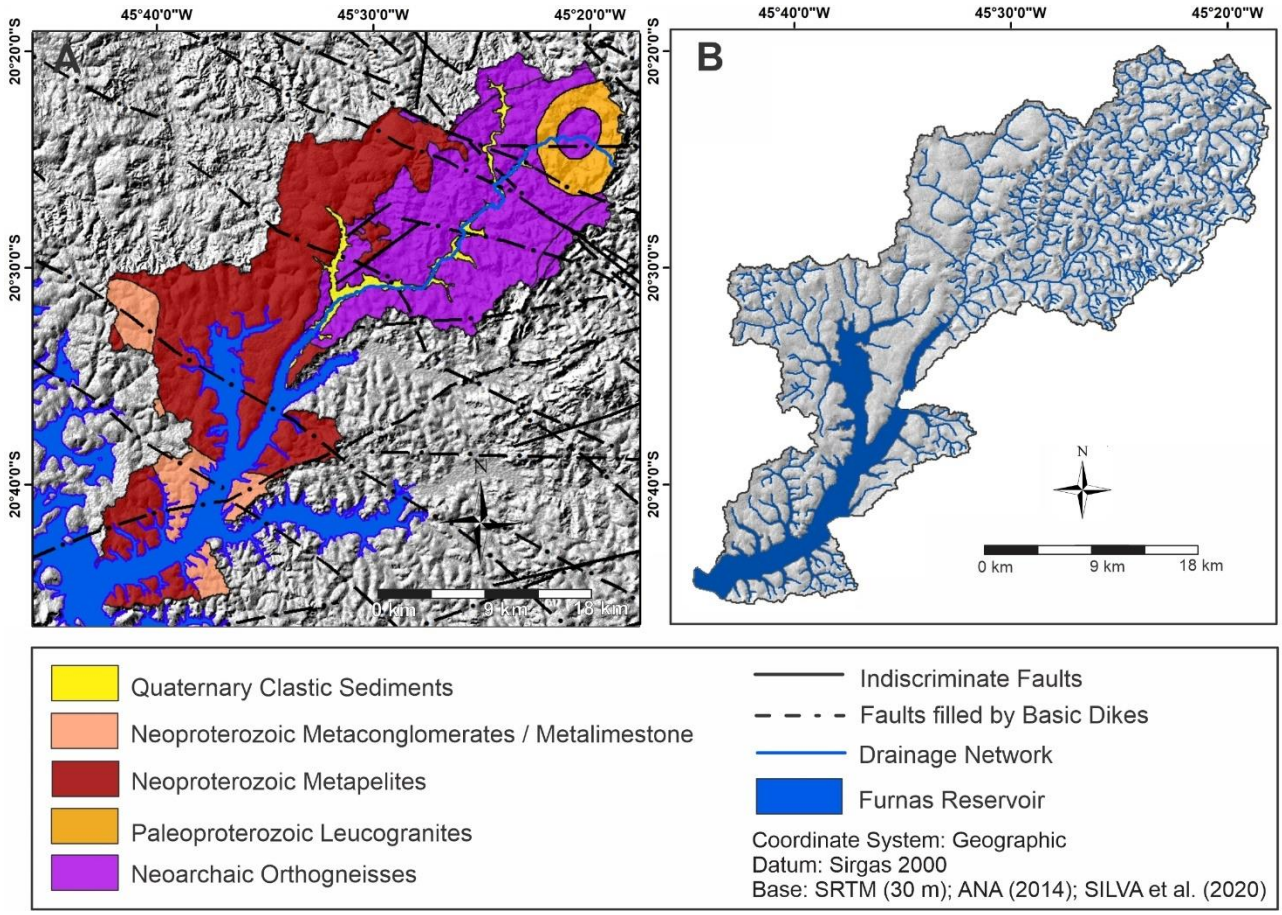

Figure 2. (A) Crystalline basement of the Proterozoic age in the upper and middle course of the river. The lower course is dominated by paraderived metamorphic rocks associated with marine transgressions and regressions that covered the São Francisco River Craton. Quaternary clastic sediments cover the alluvial segments. (B) Variation of the drainage network of the Formiga River subbasin due to the geological framework and to the reservoir of the Furnas Hydroelectric Power Plant (UHE). Adapted from Silva et al. (2020).

The soils in the area consist of Cambisols, Gleysols, Dystrophic Red–Yellow Latosols and Dystrophic Red Latosols, Dystrophic Red Ultisols, and Litholic Neosols. Cambisols and Litholic Neosols occur at the highest altitudes and slopes, while Latosols, Ultisols, and Gleysols occur at the lowest altitudes and slopes (UFV et al., 2010).

3. Materials and Methods

We obtained and processed all parameters on 30 m digital elevation model from Shuttle Radar Topography Mission (SRTM), extracted from the United States Geological Survey digital platform (free access in: http://earthexplorer.usgs.gov/) (USGS, 2023).

3.1. Drainage Anomalies and Longitudinal Profile

The longitudinal profile of the main channel was drawn from the contours of the topographic maps of Baiões (IBGE, 1969a), Formiga (IBGE, 1969b), Arcos (IBGE, 1970a), and Pontevila (IBGE, 1970b), with an equidistance of 20 m. The distances of the river segments were exported to an Excel spreadsheet. The best-fit logarithmic trend line (best line) was plotted on the longitudinal profile graph to identify the sections of the main channel with trends related to channel incision and sectors with a tendency to alluvial aggregation. Additionally,the stream length-gradient index (SL) and the normalized river steepness (Ksn) were applied to identify, quantify, and evaluate the

magnitude of drainage anomalies in the longitudinal profiles (HACK, 1973; KIRBY; WHIPPLE, 2012). The calculation of the indices involved several variables, such as: distance, amplitude, gradient, area, and concavity of the drainage subbasin (Table 1). The SL index was applied only to the main channel, while Ksn was applied to the entire drainage network.

We placed an illustrative band of the lithologies below the longitudinal profile graph to verify whether the contacts between rocks with different erosion resistances coincided with the locations of the main channel anomalies (Figure 4E). The main channel anomalies were classified according to Seeber and Gornitz (1983). We used the topotoolbox knickpoint finder tool in the MATLAB 2021a software to extract the knickpoints from the drainage network (SCHWANGHART; KUHN, 2010; SCHWANGHART; SCHERLER, 2014; 2017). We extracted knickpoints from the minimum and significant differences of 20 meters to compare the drainage anomalies identified by Ksn and SL. The curves of the topographic maps used to generate the Hack index (1973) also have an equidistance of 20 m.

Table 1. Indices used to measure drainage anomalies.

Indices	Equations	Variables	Indicative Values	References
Slope Length (SL)	$SL\ segment = \frac{\Delta H\ x\ L}{\Delta L}$ $SL\ total = \frac{\Delta Hb}{\log e\ L}$	ΔH = amplitude between the level curves, L = accumulated distance of the midpoints between the segments, ΔL = distance of the segments, ΔH_b = basin amplitude, $\log_e$ L = natural logarithm of total accumulated distance	(i) < 6 for low magnitude anomalies (1st order) (ii) > 6 for high magnitude anomalies (2nd order)	Hack (1973) Seeber and Gornitz (1983) Etchebehere et al. (2004)
Normalized river steepness (Ksn)	$Ksn = \frac{S}{A - 0ref}$	S = gradient, A = upstream drainage basin area, 0ref = reference concavity index	High values indicate ruptures along the longitudinal profile of a river	Kirby and Whipple (2012)

Subsequently, we used the point patterns on the stream network (PPS) function to classify the magnitude of the anomalies, and the Ksn function to aggregate the average values of this index in the drainage segments and in the Formiga River subbasin (SCHWANGHART; MOLKENTHIN; SCHERLER, 2021). Finally, also in MATLAB 2021a software (MATLAB, 2021), the longitudinal profiles of the entire drainage network were extracted, smoothed by the constrained regularized smoothing (CRS) function, and superimposed on the identified anomalies (SCHWANGHART; SCHERLER, 2017). We used a minimum contribution area parameter of 500 pixels to extract the drainage network. From this procedure, we derived Ksn anomaly graphs with confidence limits around the mean value per flow length.

3.2. Morphostructural parameters

We used the transverse topographic symmetry factor (T index) and the asymmetry factor of the drainage basin (AF) to assess whether the hydrographic basins suffered tectonic tilts. The application of these indices may indicate fluvial avulsion sectors from the preferential migration of the main channel due to tectonics (HARE; GARDNER, 1985; COX, 1994). The calculations of the indices involve variables related to the area of the basin and the distances between the midline of the river channel and the interfluves (Table 2). Global Mapper 23 software (GLOBAL MAPPER, 2022) prepared topographic profiles transversal to the fluvial valleys to show the morphology resulting from fluvial migration.

Table 2. Indices used for morphostructural measurements.

Indices	Equations	Variables	Indicative Values	References
AF	$AF = 100\frac{Ar}{At}$	Ar = Right basin area in km² At = Total area of the basin in km²	(i) < 50 reveals little or no tectonic activity (ii) > 50 indicates possible tilting	Hare and Gardner (1985)
T	$T = \frac{Da}{Dd}$	Da = distance from the midline of the basin axis to the main channel in km Dd = distance from the midline to the watershed divider closest to the current course of the river in km	(i) Close to 0.0 reflects symmetrical stretches with little lateral displacement of the river in relation to the mean axis (ii) Close to 1.0 indicates a greater degree of asymmetry of the sections in relation to the average axis (tilting)	Cox (1994)

We mapped structural lineaments to identify the areas most affected by deformational events and the sectors most susceptible to tectonic reactivations. For extraction we applied in the DEM shading from solar positioning simulations in based on azimuths of 315°, 360°, 45°, and 90° (CORRÊA; FONSÊCA, 2010). In addition, we exported the hillshades files from ArcGis 10.8 (ESRI, 2020) for PCI Geomatics software 2016 (PCI GEOMATICS, 2016), where we extracted the lineaments automatically. Then, we performed manual validation by checking the duplicity of lineaments or associated errors. Afterward, we imported the shapes of the extracted lines into ArcGIS 10.8, where we elaborated the lineament density map using the Kernel Density tool, with a definition of 5 density classes. Finally, we created the rosette diagram using RockWorks17 software (ROCKWARE, 2016) applying the geographic coordinates relative to the ends of the extracted lines.

3.3. Relief morphometric parameters

The relief ratio (Rr) is the ratio between the altimetric amplitude of the basin and the length of the main channel, and the bigger Rr is, the greater the difference in the level and the average slope of the basin (SCHUMM, 1956) (Table 3). The roughness index (Ir) relates the slope and the lengths of the channels; high index values indicate the presence of hilly relief, dissected with more notched channels (MELTON, 1957; HOBSON, 1972; SOUSA; RODRIGUES, 2012).

Table 3. Relief morphometric parameters.

Indices	Equation	Variables	Indicative Values	References
Relief Ratio (Rr)	$Rr = \frac{Hm}{Lc}$	Hm = altimetric amplitude of the basin in m Lc = length of the main channel in km	(i) < 10.00 m km^{-1} (low ratio) (ii) 10.00 - 30.00 m km^{-1} (average ratio) (iii) 30.00 - 60.00 m km^{-1} (high ratio) (iv) > 60.00 m km^{-1} (very high ratio)	Schumm (1956) Piedade (1980)
Roughness Index (Ir)	$Ir = Hm\,.\,Dd$	Hm = altimetric amplitude of the basin in m Dd = drainage density in km km^{-2}	(i) < 150.00 (low roughness) (ii) 150.00 - 550.00 (average roughness) (iii) 550.00 - 950.00 (high roughness) (iv) > 950.00 (very high roughness)	Melton (1957) Hobson (1972) Sousa and Rodrigues (2012)

The local roughness concentration index (Icr) aims to quantify and classify roughness patterns based on slope variations (SAMPAIO, 2008; SAMPAIO; AUGUSTIN, 2014). The steps to obtain the Icr involved procedures related to (i) measurement of the matrix slope obtained from the DEM; (ii) conversion of the matrix product into vectors; (iii) application of kernel density algebra (1 km²); (iv) data normalization by dividing the values obtained by the number of pixels computed; and (v) categorization of classes (SAMPAIO; AUGUSTIN, 2014). The values of these indices vary from close to zero for predominantly flat areas with high interfluvial dimensions and a low degree of

vertical carving to approximately infinity for areas with very uneven relief with low interfluvial dimensions and a high degree of vertical carving.

3.4. Morphometric parameters of the drainage network

The river hierarchy establishes the orders of river channels and relationships with the capacity of springs (STRAHLER, 1952). The drainage density (Dd) and the hydrographic density (Dh) indicate relationships between the average length of channels per unit area, the concentration of water courses, the water infiltration capacity, the contribution to water table supply, and the capacity to generate new water flows, in addition to expressing the degree of topographic dissection promoted by the fluvial action (HORTON, 1945). The sinuosity index (Is) expresses the flow velocity of the main channel, in addition to determining the characteristics of the pattern: straight, sinuous, or meandering (HORTON, 1945; SCHUMM, 1963; MANSIKKANIEMI; 1970) (Table 4). We determined the stream order extracting the drainage network from DEM by the hydrology function in ArcGis 10.8 (ESRI, 2020).

Table 4. Morphometric parameters of the drainage network.

Indices	Equations	Variables	Indicative Values	References
Hydrographic Density (Dh)	$Dh = \frac{n}{A}$	N = total number of channels A = basin area in km²	(i) < 3 (low density) (ii) 3 - 7 (average density) (iii) 7 - 15 (high density) (iv) > 15 (very high density)	Horton (1945) Lollo (1995)
Drainage Density (Dd)	$Dd = \frac{Lt}{A}$	Lt = total length of channels in km A = basin area in km²	(i) < 0.5 (very low density) (ii) 0.5 - 1.5 (low density) (ii) 1.5 - 2.5 (average density) (iii) 2.5 - 3.5 (high density) (iv) > 3.5 (very high density)	Horton (1945) Villela e Mattos (1975)
Sinuosity Index (Is)	$Is = \frac{100\ (L - Lt)}{L}$	L = length of the main channel in km Lt = vector length of the main channel in km	(i) < 20% (very straight channel) (ii) 20.0 - 29.9% (straight channel) (iii) 30.0 - 39.9% (rambling channel) (iv) 40.0 - 49.9% (sinuous channel) (v) > 50% (very sinuous channel)	Horton (1945) Mansikkaniemi (1970)

3.5. Morphometric parameters of the basin

The compactness coefficient, circularity index, and form factor establish geomorphological and hydrological relationships regarding the shape of hydrographic basins and the tendency of floods to occur (Table 5) (SCHUMM, 1956; VILLELA; MATTOS, 1975). These indices have the same concept and interpretation. Higher values indicate that the basin tends to be more circular, favoring flooding processes (Table 5). Variables previously calculated for the other parameters were used for the calculation, except for the perimeter of the basin.

Table 5. Basin morphometric parameters.

Indices	Equations	Variables	Indicative Values	References
Compactness Coefficient (Kc)	$K = 0.28\ x\ \frac{\mathrm{P}}{\sqrt{\mathrm{A}}}$	P = Basin perimeter in km A = Basin area in km²	(i) 1.0 - 1.25 (high propensity to flooding) (ii) 1.26 - 1.50 (average trend) (iii) > 1.50 (not subject to large floods)	Gravelius (1914) Villela e Mattos (1975)
Circularity Index (Ic)	$IC = 12.57\ x\ \frac{\mathrm{A}}{\mathrm{P}^2}$	P = Basin perimeter in km A = Basin area in km²	(i) > 0.51 (favoring flooding) (ii) < 0.51 (favoring flow)	Miller (1953) Schumm (1956)
Form Factor (Ff)	$Ff = \frac{\mathrm{L}}{\mathrm{B}}$	L = average basin width in km B = Axial length of the basin in km	(i) ≥ 0.75 (basin subject to flooding) (ii) 0.75 - 0.50 (average trend) (iii) ≤ 0.50 (basin not subject to flooding)	Gravelius (1914) Horton (1945)

4. Results

The normalized channel steepness index application shows stretches with high Ksn values in the upper and middle course of the main Formiga River channel (Figure 3A) in areas of higher altitudes, close to the main drainage headwaters (Figure 3B). However, the distribution of mean values of Ksn by flow length among all tributaries generally indicates a drainage network that mostly presents a low erosive gradient domain, especially in the lower course (Figure 3C). The concavity index shows the relationship between slope and area and points to the relative dispersion of small tributaries adjacent to the lower course of the Formiga River and emptying into the Furnas Reservoir (Figure 3D). The observed pattern results in a few significant breaks greater than 20 m, totaling 7 knickpoints (Figures 3E and 3F).

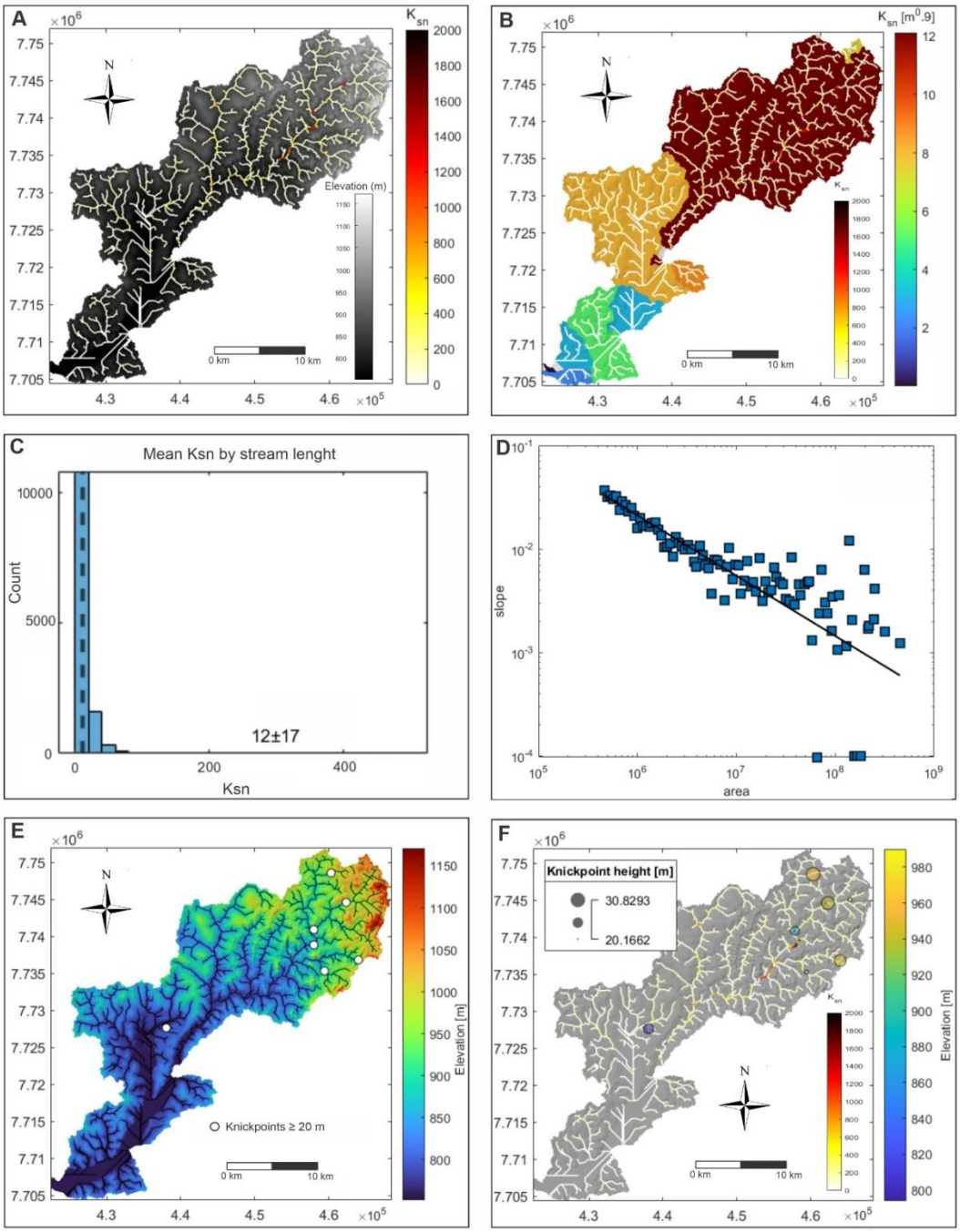

Figure 3. (A) Ksn values of the drainage network. (B) Mean Ksn values of the subbasin. (C) Knickpoints ≥ 20 m. (D) Classification of the magnitude of knickpoints ≥ 20 m. (E) Calculation of the concavity index using the slope area function. (F) Mean Ksn by flow length showing the distribution of Ksn values of pixels, mean and standard deviation (12 ± 17).

Among the identified knickpoints, three are located on the main river, three are linked to the tributaries of the middle course, and one is linked to the lower course (Figures 4A and 4B). The deformations in the main channel are associated with the positive anomalies of the original DEM, with narrower acceptance intervals toward the upstream, a fact that reduces the uncertainties of the Ksn values and increases the reliability of the data (Figure 4C). The average elevation angle of the slopes adjacent to the upper and middle river courses present greater dispersion when compared to the lower course due to the greater slopes and roughness of the terrain in the upstream sectors (Figure 4D). Such main channel anomalies are also identified by the stream length gradient, which demarcates the transition between the upper, middle, and lower courses of the river and shows sectors with a tendency of erosive readjustments upstream (Figure 4E).

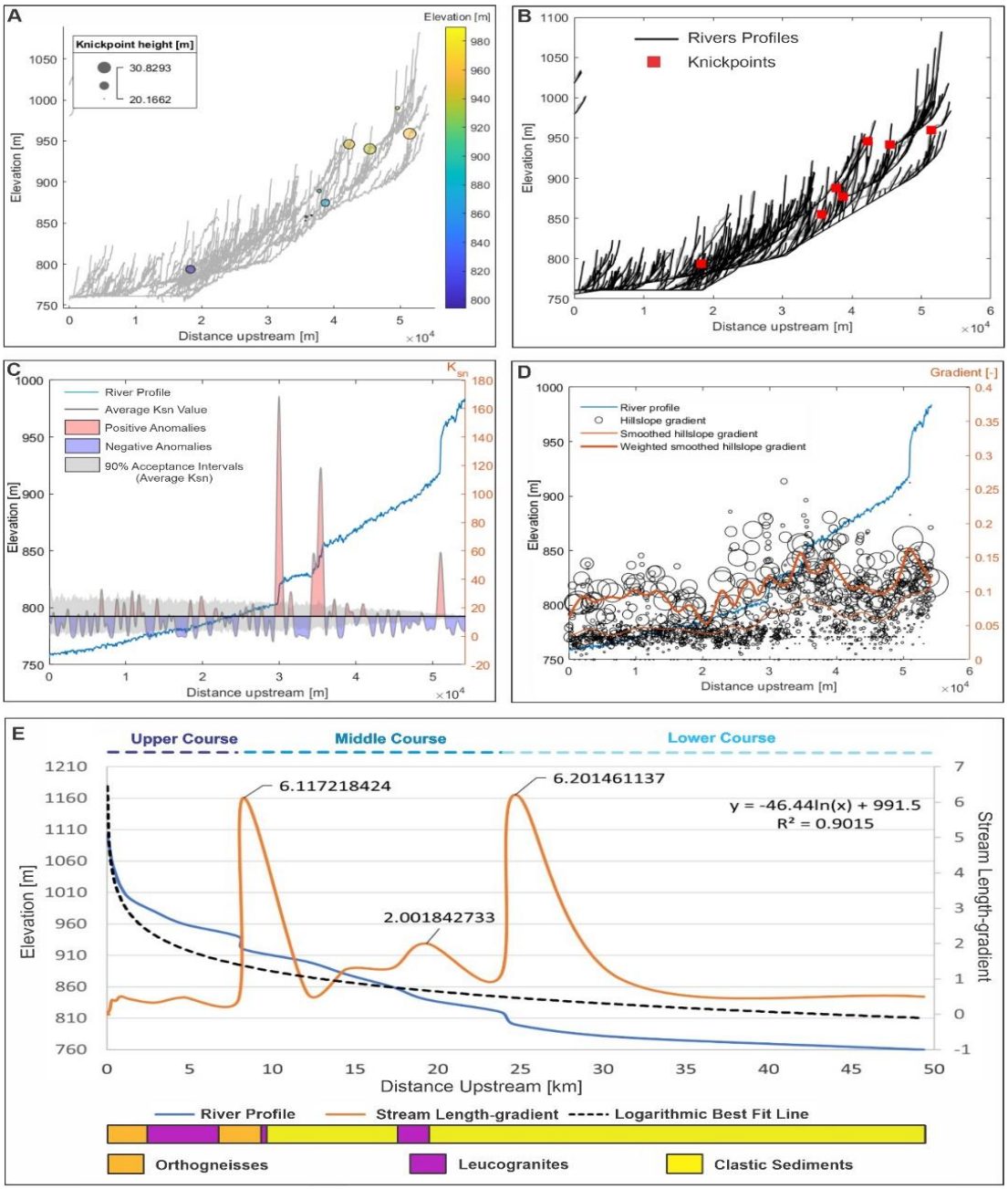

Figure 4. (A) Longitudinal profiles extracted based on a minimum slope area of 500 pixels and location and magnitude of the knickpoints. (B) MDE smoothing, hydrological normalization of profiles and anomalies. (C) Acceptance intervals showing the uncertainties of the Ksn values of the main river. (D) Average angle of elevation of the slopes of the main river, showing the dispersion of the gradient. (E) Longitudinal profile, knickpoints, and values obtained by the SL index, correlated with lithology and logarithmic curve of best fit upstream.

The first anomaly found in the river's upper course has a structural genesis, reflecting 2nd-order deformation, and is located near the contact of rocks with different erosive resistances (leucogranites and orthogneisses) (Figures 2A and 4E). The second anomaly located in the middle course has a structural genesis (Figures 5A and 5C), indicating 1st-order deformation between faults filled by basic dikes and in a contact zone between orthogneisses with greater mechanical resistance to removal and clastic sediments (Figures 2A and 4E). The third anomaly identified (Figures 5B and 5C) has tectonic genesis adjacent to a fault zone (Figure 2A) and is associated with 2nd-order deformation (Figures 2A and 4E).

Figure 5. (A) Knickpoint 2 with structural genesis. (B) Knickpoint 3 with tectonic genesis. (C) Three-dimensional model of the surroundings of the urban center of Formiga showing the river sections with knickpoints.

Regarding the morphostructural parameters, the density of structural lineaments indicates the concentration in the upstream sector of the subbasin, which suggests the greater performance of deformational events in drainage anomalies in places with high slopes, rougher relief/hills, and geological substrate with greater resistance to erosion (Figures 6A and 6B). The central and downstream sectors of the Formiga River subbasin have a lower density of

structural lineaments, smoother slopes, and relatively flat relief that reflect the lower incidence of tectonic deformation activities (Figures 6A and 6B). These sites are more likely to deposit than export sediment. The rosette diagram shows the preferential orientation of tectonic activities trending predominantly NW–SE (315°/135°) (Figure 6A).

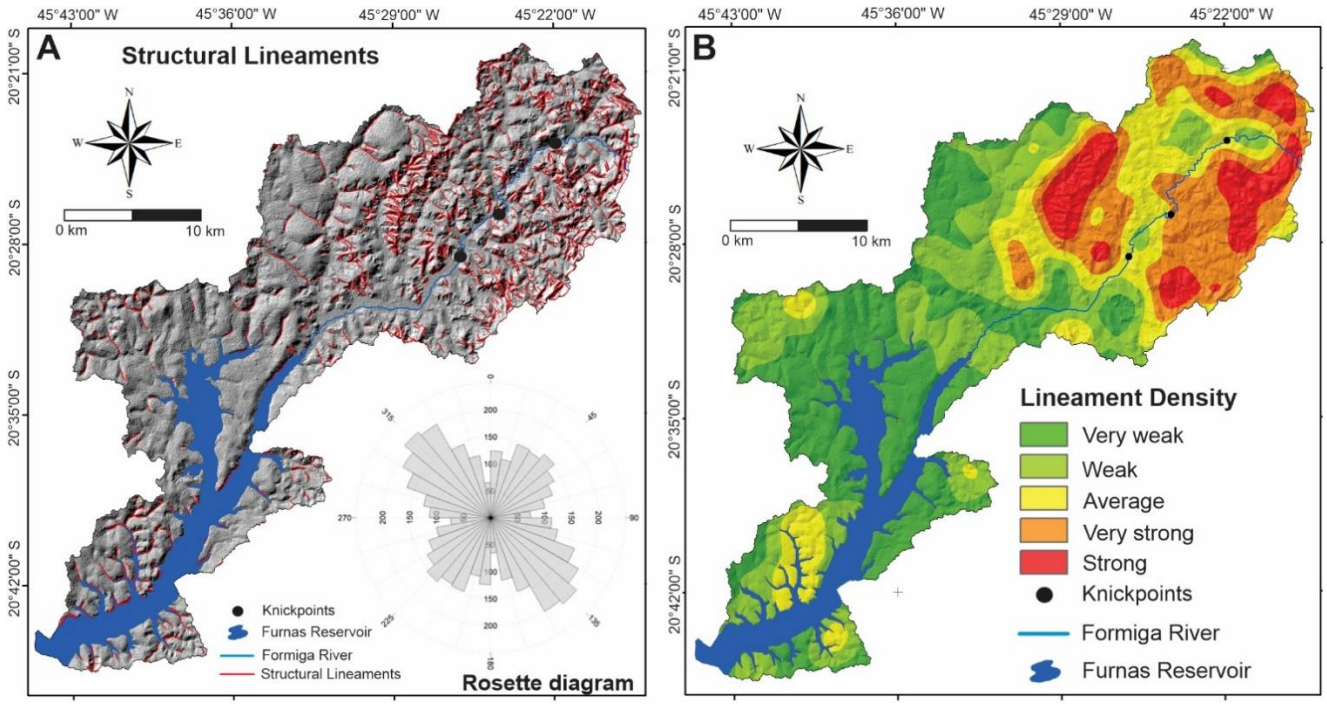

Figure 6. (A) Structural lineaments of the Formiga River subbasin and rosette diagram showing the preferential direction and frequency of the lineaments. (B) Map of density of lineaments.

An AF of 69.28 indicates tectonic activity in the Formiga River subbasin, with a tendency of preferential tilting toward the eastern sector (Figure 7). The embedded pattern of the upper and middle courses makes the lateral displacement of the watercourse difficult. Downstream, on the contrary, with a course in an alluvial bed with wide plains, the river presents a pattern of lateral displacement due to the lower resistance imposed by lithological and tectonic conditions. Such results are corroborated by the T index data, which indicate significant and nonuniform relief tilting (Figure 7). The upper and middle courses present values close to 0, typical of symmetrical sections with little lateral displacement of the channel. In contrast, the lower course presents values close to 1.0, which indicates greater asymmetry of this stretch due to tilting and less resistance to avulsion offered by the alluvial beds. The remainder of the drainage network also reflects eastward tilting, with lower-order river channels in the western sector being longer than the eastern channels (Figures 8A, 8B, and 8C).

The hydrographic density showed a value related to 0.69 channels km^{-2}, indicating the low capacity to generate new rivers in the current geomorphological and lithological configuration of the subbasin. The drainage density also has low values, on the order of 1.19 channels km^{-2}, which suggests a low infiltration capacity of surface water. On the other hand, the sinuosity index measured in the main watercourse has a value of 0.43%, which indicates a very straight channel with significant surface runoff velocity.

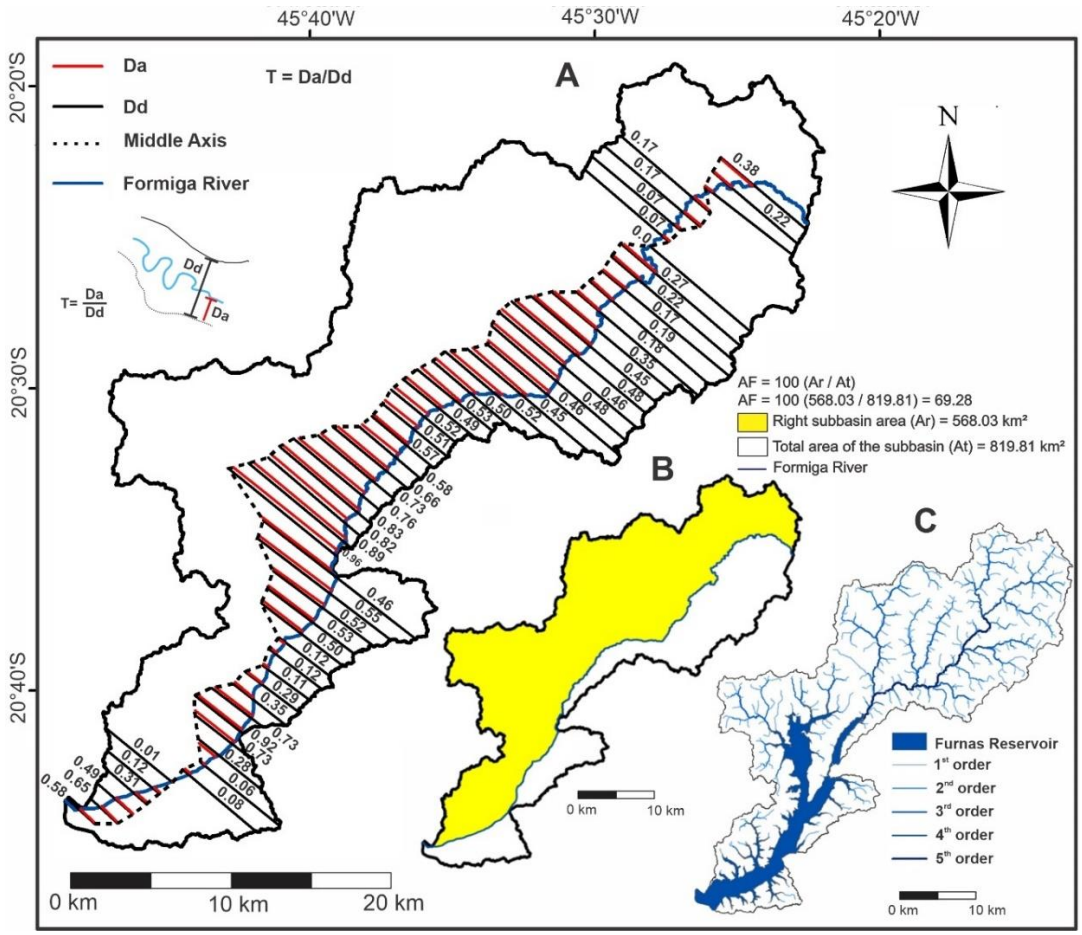

Figure 7. (A) Transverse topographic symmetry factor. (B) Asymmetry factor. (C) Stream order.

The Dh and Dd values are derived from the average of the entire subbasin, and thus, geoprocessing was carried out to verify the distribution. The individualization of the sectors shows that the highest values are concentrated upstream due to the rocks being characterized by greater resistance to water infiltration. This relationship indicates the capacity of loading and storage of the subsurface flow, since the individualized data suggest that the greatest contribution to groundwater supply occurs in the lower course (Figures 8A and 8B).

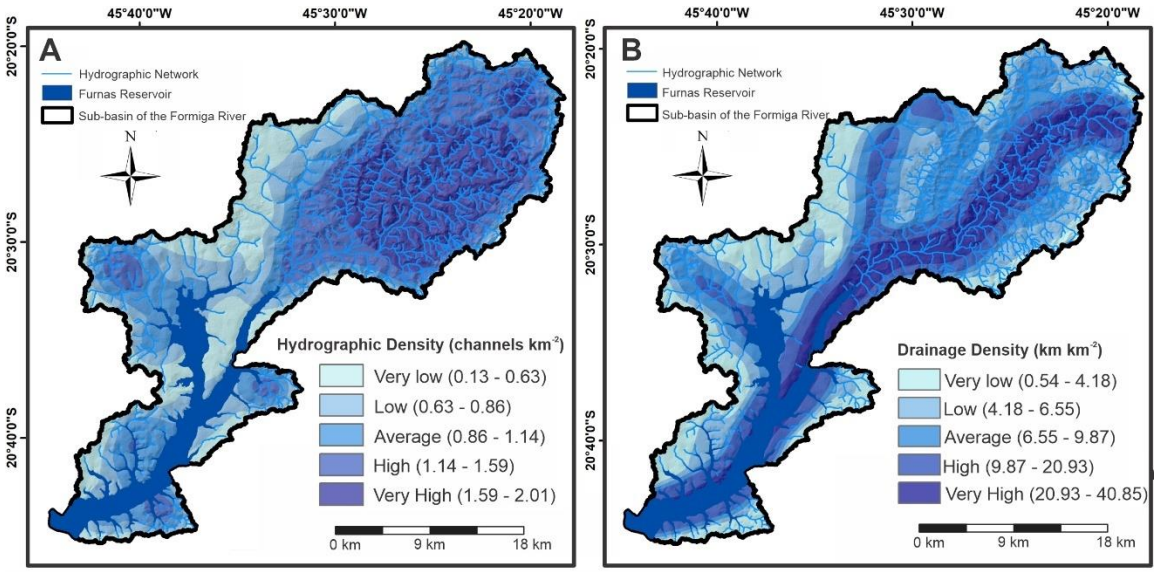

Figure 8. (A) Hydrographic density. (B) Drainage density of the Formiga River subbasin.

The values related to the relief ratio (Rr) and roughness index (Ir) reveal a low relief ratio (8.5 m km^{-1}) and average terrain roughness (498.61 m km^{-2}), respectively. This indicates that the Formiga River subbasin has little difference in level. As the values of these indices are derived from the average obtained for the entire extension of the basin, the roughness concentration index (Icr) is also applied to identify the distribution on the terrain. The individualization of the sectors (Figure 9A), calibrated by the slope of the terrain (Figure 9B), shows that the highest values are associated with the main drainage headwaters in the upper and middle courses. The medium and low values are downstream, at the confluence with the reservoir of the UHE de Furnas (Figure 9A). Furthermore, topographic profiles transversal to the river valleys allowed interpretations from the correlation with the morphostructural, morphometric, and morphological parameters (Figure 9C). The roughest topographic pattern occurs where the river is embedded in the rocky substrate, in stretches with low T index values and a high density of structural lineaments (Profile A-A'). The other profiles (B-B', C-C', D-D', and E-E') elucidate the asymmetry of the slopes in the lower course (higher values of FSTT), arranged between terrains of lower roughness and low density of lineament structures. This result illustrates the greater lateral displacement of the river in the alluvial bed and the reflections on the erosive/depositional balance of the transported sedimentary load. The last profiles show the importance of natural conditioning for water storage related to the Furnas Reservoir in the hydrographic subbasin (D-D' and E-E') (Figure 9C).

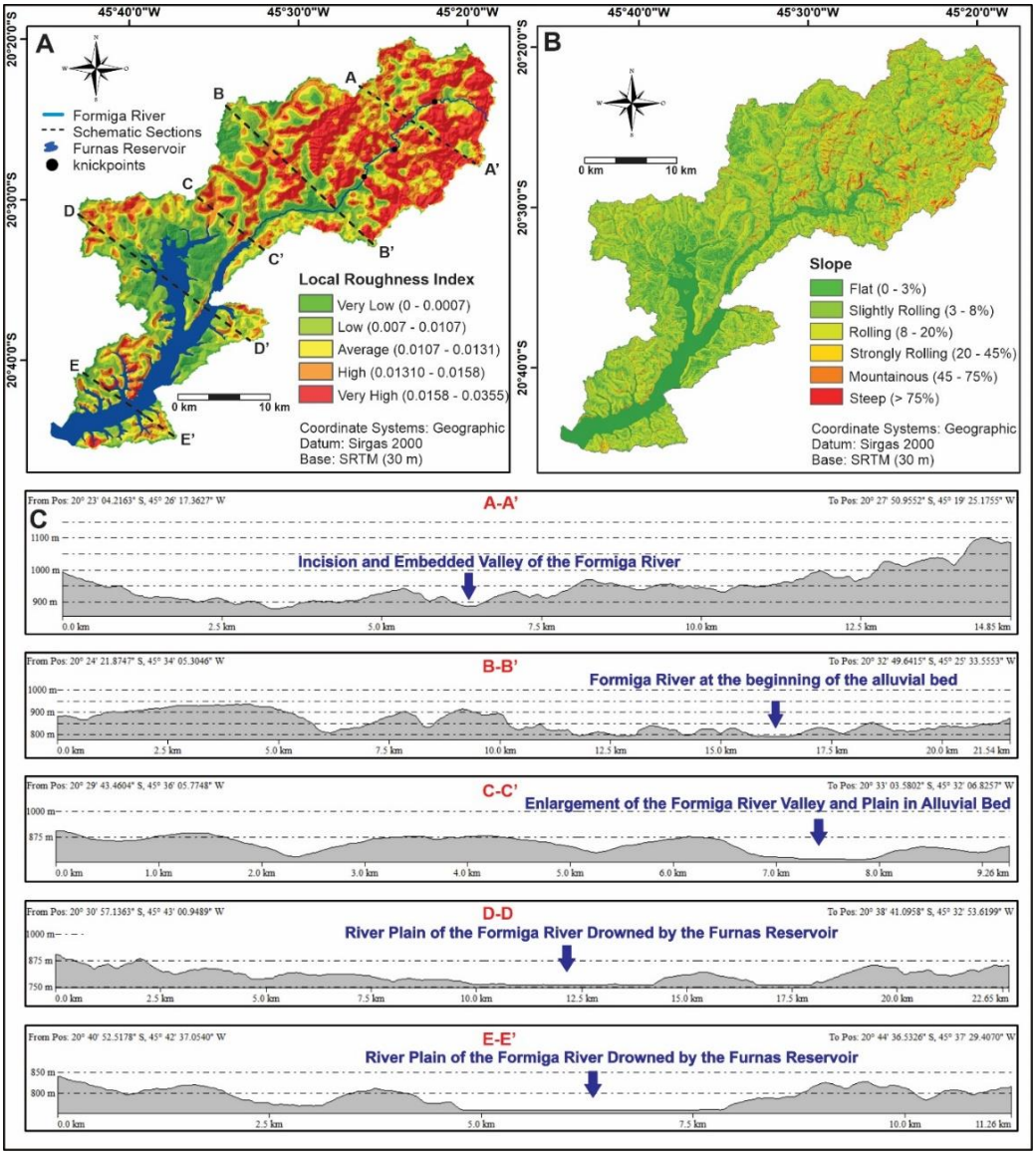

Figure 9. (A) Roughness concentration index. (B) Slope. (C) Schematic sections transverse to the valley of the main channel between basin interfluves (A-A', B-B', C-C', D-D', and E-E').

Finally, the application of the compactness coefficient (Kc), circularity index (Ic), and form factor (Ff) reveal that the subbasin (i) is not subject to large floods (Kc = 2.36); (ii) the occurrence of runoff processes to the detriment of floods is favorable (Ic = 0.17); and (iii) it has a considerable concentration time during rainy peaks (Ff = 0.20). The geometry of the subbasin is composed of a dendritic drainage network with an elongated shape (Figure 10).

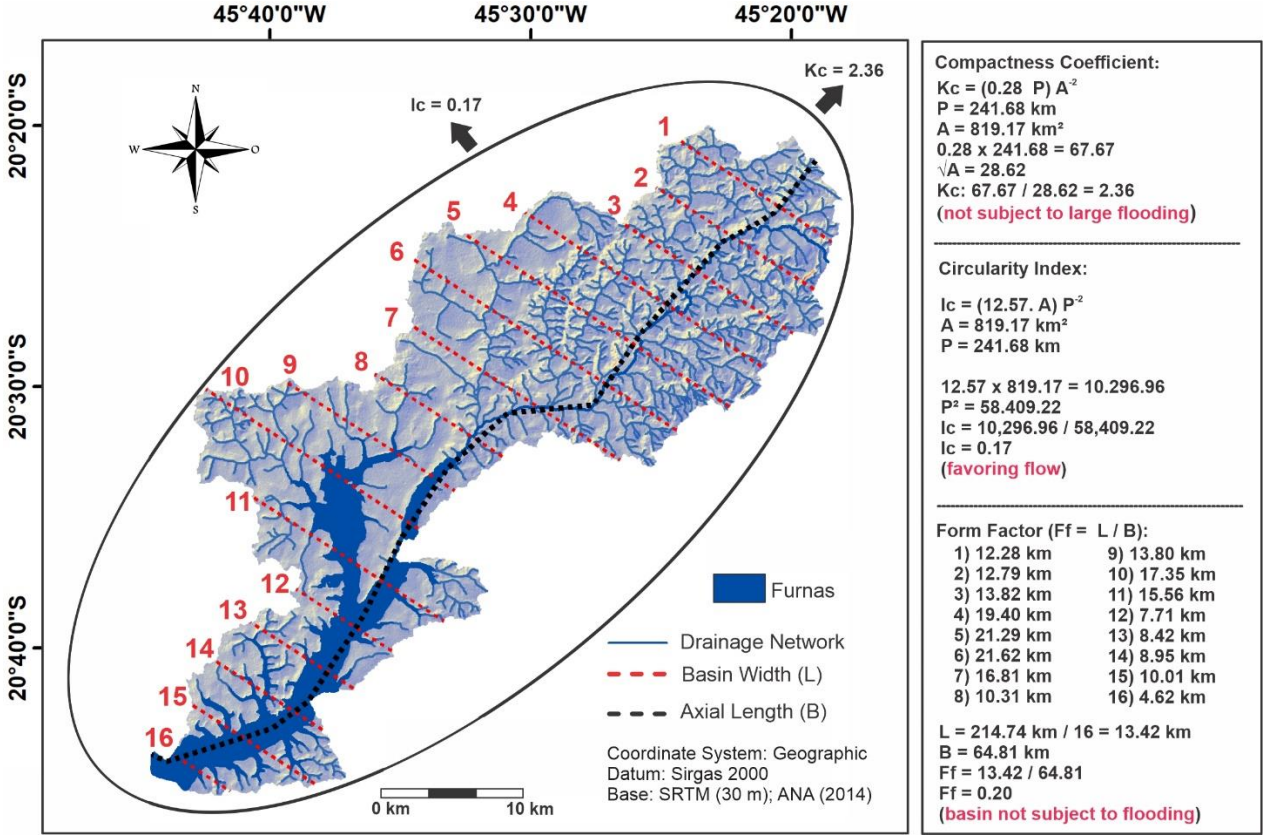

Figure 10. Compactness coefficient, circularity index, and form factor of the Formiga River basin.

5. Discussion

The integrated analysis of morphological and morphometric parameters resulted in the identification of three sectors of the subbasin that reflect distinct geomorphic behaviors. The upstream sector, represented by the upper and middle course of the Formiga River, characterized by igneous and metamorphic rocks with greater erosion resistance and density of structural lineaments, points to a greater performance of deformation events and greater susceptibility to the occurrence of neotectonic reactivations. This interpretation is supported by Bhattacharjee et al. (2013), who also recognized the importance of integrating these parameters for the design and notes on neotectonic activities. These authors mapped known fault zones and tectonic lineaments of the central Indian craton, from which it was possible to understand the nature and tectonic and structural behavior of the Indian Peninsula.

The lithostructural and tectonic configuration of this upstream sector provides a greater concentration of surface water at the expense of subsurface water supply induced by infiltration. When comparing the maps referring to the fluvial hierarchy, drainage density, and hydrographic density, it is possible to notice this relationship. Different authors have investigated these correlations on local, regional, and global scales (TUCKER et al., 2001; HAN et al., 2003; LAZZARO; ZARLENGA; VOLPI, 2015; SCHNEIDER et al., 2017; LIN et al., 2021). The results of these studies also converge to a dependence between the variability of surface runoff yield and infiltration due to the heterogeneity of Dh and Dd, working with an indicator that reflects the local climate, relief, and geology of the area and is therefore capable of elucidating the marks of active tectonics in river systems. All these conditions influenced the relief development, in which the upstream area has a sloping and very rough pattern due to the dissections imposed by the river courses, which are mostly embedded in the rocky substrate. The low values of the T index in the upper and middle courses corroborate these interpretations, since they presented symmetrical stretches with little lateral displacement of the river in relation to the middle axis.

The application of the normalized channel steepness index showed that this stretch is also characterized by the highest values of Ksn of the drainage network, where six knickpoints with amplitudes greater than 20 m occur, three of them on the main channel. This reflects the constant attempt to readjust the drainage network in the face of natural disturbances, recurrent in the deformational regions adjacent to the Mantiqueira mountain range (SANTOS; TASSINARI; FONSECA, 2015; CALEGARI et al., 2021; KURIBARA et al. 2019) and the San Francisco Craton (BRUNO et al., 2020; CUTTS et al., 2020; FONSECA et al., 2021). The dynamics related to nonlinear fluvial readjustments show that the rivers are not static and that the disturbance results from i) cumulative responses to recent events; (ii) delayed responses to past events; and/or (iii) external responses to events that occurred in other places (DUNCAN, 2015).

Souza et al. (2022) also highlighted the importance of applying morphometric indices and the resulting results to strengthen neotectonic interpretations on passive continental margins. The authors sought to understand the landforms, drainage systems, and hydrographic basins of the continental margin of Northeast Brazil based on the application of geomorphic indices used in the present study (SL, Ksn, and T index). The use of such methods provided robust evidence of regional tectonic control by proving high values associated with fault zones, which confined and directed drainage and landforms. Such dynamics conditioned the longitudinal profiles of the rivers, which, due to their morphology, triggered natural disturbances that affected the basins (DUNCAN, 2015; SOUZA et al., 2022).

The central sector of the Formiga River subbasin presents a transition between rocks of greater (orthogneisses) and lesser resistance to erosion (metapelites/metalimestones) in places with low concentrations and frequencies of structural lineaments, indicating that this sector was less affected by the action of deformational events. The lithostructural and tectonic configuration of this sector favors the infiltration processes to the detriment of the higher concentration of surface water, giving lower values of hydrographic density of the subbasin. It also provided a greater capacity for lateral migration of the river, according to the asymmetry due to tectonic forces (tilting) and low resistance to the avulsion of the alluvial beds. According to the topographic profiles, these structural, and water dynamics developed relief surfaces with convex and recessed tops, with long, slightly rolling slopes and wide river plains (Figure 9). The application of the normalized channel steepness index in this sector illustrates a drainage network that presents a predominance of a low erosive gradient, especially in the lower course, which shows a pattern of only one significant rupture greater than 20 m. It is important to note that the resistance of rocks to erosion is a factor frequently described in geomorphic studies and, generally, strongly affects the shape of the relief (AUGUSTINUS, 1991). Critelli et al. (2015), Smeraglia et al. (2021), and Omidiji et al. (2022) examined the resistance properties of several types of carbonate rocks. They considered the high propensity of these terrains to infiltration potentiated by chemical dissolution and a decrease in surface water capacity. At the same time, the application of indices such as the T index and AF are increasingly being used to investigate the effects of tilting on drainage networks and geomorphological configurations of basins (GOSWAMI; PANT, 2019; RADAIDEH; MOSAR, 2019; GIMENEZ et al., 2022; MITROFAN et al., 2022; MAKRARI et al., 2022). In particular, Ouchi (1995) and Garrote et al. (2006) established dynamic relationships between the slope of the surface, lateral migration of the channel in an alluvial bed (parallel to its original course), and adaptation to the steepest gradient.

Finally, the sector downstream of the basin, close to the confluence with the Grande River (MG), is composed of medium (metaconglomerates) to low resistance (metapelites/metalimestones) rocks in regard to erosion, which explains the variation in terrain roughness, relief slope, and hydrographic density and the concentration of structural lineaments observed at the site. No significant knickpoint was found in the drainage network, which was composed of null values of Ksn. In this sector, there is the Furnas Reservoir, which floods a large part of the wide river plains of the lower course, with a slight increase in the hydrographic density in the transition areas between the lithotypes, possibly due to the greater difficulty of infiltration in the fault/joint/fracture planes. Smeraglia et al. (2021), while investigating the massive Monte Alpi in Italy, established similar correlations, concluding that clay scattered along fault segments of shales and metapelites resulted in low permeability zones. The fault intersections in the limestones have high permeability in the central and downstream sectors of the Formiga River subbasin.

For the migration of the fluvial channel, the reduction in the T index values in relation to the mean axis is remarkable, which shows the nonuniform tectonic tilting of the subbasin, restricted to significant tilted blocks in the central sector. The Furnas Reservoir, responsible for the drowning of the lower course, shows a high influence

on the current water and ecosystem dynamics. The impacts of these types of interventions are well documented in the scientific literature (ARANTES et al., 2019; HUNT et al., 2020; SZMAŃDA et al., 2021; PETTS; GURNELL, 2022).

6. Conclusions

The analysis of the morphostructural, morphological, and morphometric parameters of the hydrographic subbasin of the Formiga River proved to be effective in characterizing and understanding the structure and geomorphic configuration of the basin. The methodology used proved to be efficient and can be replicated for analysis in other areas. The integration between the indices proposed by the literature in the 20th century, with the new methods developed in the last decade, was successful in the investigation of the control mechanisms acting in the hydrographic subbasin of the Formiga River.

The integrated analysis of the parameters revealed three sectors of the hydrographic subbasin with distinct geomorphic behaviors, resulting in surface structures with divergent current dynamics. The subbasin presents concrete evidence that corroborates a strong indication of structural control in developing of the drainage network and relief.

Human action, added to natural factors, has also influenced the current relief/drainage configuration, mainly related to the drowning of the lower river course, induced by the development of the Furnas Reservoir. The construction of dams adjacent to the urban core of the Municipality of Formiga intensified the retention of sediments and altered the erosive/depositional dynamics of the sedimentary balance of the main channel downstream.

Author's contributions: Writing, data preparation and original draft preparation, I.L.R and G.S.M.; review and editing, G.S.R., D.B.S. and G.H.E.L.; conception, writing and review, R.L.M and F.G.R.; supervision F.G.R. All authors have read and agreed to the published version of the manuscript.

Funding: This research has not received any external funding

Acknowledgments: Thanks to "Fundação de Amparo à Pesquisa do Estado de Minas Gerais (FAPEMIG)" for scholarships to the second and fifth author; to the "Coordination for the Improvement of Higher Education Personnel - Brazil (CAPES)" for the third author's scholarship and to "Ipanema Agrícola S.A." for the scholarship of the fourth author.

Conflict of Interest: The authors declare no conflict of interest.

References

1. ALMEIDA, W. S.; SOUZA, N. M.; REIS JUNIOR, D. S.; CARVALHO, J. C. Análise morfométrica em bacias hidrográficas fluviais como indicadores de processos erosivos e aporte de sedimentos no entorno do reservatório da usina hidrelétrica (UHE) Corumbá IV. **Revista Brasileira de Geomorfologia,** v. 14, n. 2, p. 135-149, 2013. DOI: 10.20502/rbg.v14i2.251

2. ALVARES, C. C.; STAPE, J. L.; SENTELHAS, P. C.; GONÇALVES, J. L. M.; SPAROVEK, G. Köppen's climate classification map for Brazil. **Meteorologische Zeitschrift,** v. 22, n. 6, p. 711-728, 2014. DOI: 10.1127/0941-2948/2013/0507

3. ALVES, F. C.; ROSSETTI, D. F.; VALERIANO, M. M. Detecting neotectonics in the lowlands of Amazonia through the analysis of river long profiles. **Journal of South American Earth Sciences**, v. 100, 102553, p. 1-11, 2020. DOI: 10.1016/j.jsames.2020.102553

4. ALVES, F. C.; STOKES, M.; BOULTON, S. J.; ROSSETTI, D. F.; VALERIANO, M. M. Post-rift geomorphological evolution of a passive continental margin (Paraíba region, northeastern Brazil): Insights from river profile and drainage divide analysis. **Geomorphology**, v. 414, 108384, p. 1-18, 2022. DOI: 10.1016/j.geomorph.2022.108384

5. ANA. **Base Hidrográfica Ottocodificada da Bacia do Rio Grande.** Brasília: ANA, 2014. Escala 1:50.000. Disponível em: < https://metadados.snirh.gov.br/geonetwork/srv/api/records/b13fa102-148d-4c4a-b7cd-02f23027e5c1>. Acesso em: 19 out. 2022.

6. ARANTES, C. C.; FITZGERALD, D. B.; HOEINGHAUS, D. J.; WINEMILLER, K. O. Impacts of hydroelectric dams on fishes and fisheries in tropical rivers through the lens of functional traits. **Current Opinion in Environmental Sustainability,** v. 37, n. 1, p. 28-40, 2019. DOI: 10.1016/j.cosust.2019.04.009

7. AUGUSTINUS, P. C. Rock resistance to erosion: some further considerations. **Earth Surface Process and Landsforms,** v. 16, p. 563-569, 1991. DOI: 10.1002/esp.3290160608

8. BARROS, L. F.; REIS, R. A. P. A produção científica em geomorfologia fluvial na Revista Brasileira de Geomorfologia: panorama bibliográfico, tendências e lacunas. **Revista Brasileira de Geomorfologia,** v. 20, n. 3, p. 673-680, 2019. DOI: 10.20502/rbg.v20i3.1553

9. BHATTACHARJEE, D.; JAIN, V.; CHATTOPADHYAY, A.; BISWAS, R.H.; SINGHVI, A.K. Geomorphic evidences and chronology of multiple neotectonic events in a cratonic area: Results from the Gavilgarh Fault Zone, central India. **Tectonophysics,** v. 677-678, p. 199-217, 2016. DOI: 10.1016/j.tecto.2016.04.022

10. BRUNO, H.; ELIZEU, V.; HEILBRON, M.; VALERIANO, C. M.; STRACHAN, R.; FOWLER, M.; BERSAN, S.; MOREIRA, H.; DUSSIN, I.; EIRADO SILVA, L. G.; TUPINAMBÁ, M.; ALMEIDA, J.; NETO, C.; STOREY, C. Neoarchean and Rhyacian TTG-Sanukitoid suites in the southern São Francisco Paleocontinent, Brazil: Evidence for diachronous change towards modern tectonic. **Geoscience Frontiers,** v. 11, n. 5. p. 1763-1787, 2020. DOI: 10.1016/j.gsf.2020.01.015

11. CALEGARI, S. S.; PEIFER, D.; NEVES, M. A.; CAXITO, F. A. Post-Miocene topographic rejuvenation in an elevated passive continental margin not characterized by a sharp escarpment (northern end of the Mantiqueira Range, Brazil). **Geomorphology,** v. 393, 107946, 2021. DOI: 10.1016/j.geomorph.2021.107946

12. CALIL, P. M.; OLIVEIRA, L. F. C.; KLIEMANN, H. J.; OLIVEIRA, V. A. Caracterização geomorfométrica e do uso do solo da Bacia Hidrográfica do Alto Meia Ponte, Goiás. **Revista Brasileira de Engenharia Agrícola e Ambiental,** v. 16, n. 4, p. 433-442, 2012. DOI: 10.1590/S1415-43662012000400014

13. CASTILLO, M.; BISHOP, P.; JANSEN, J. D. Knickpoint retreat and transient bedrock channel morphology triggered by base-level fall in small bedrock river catchments: The case of the Isle of Jura, Scotland. **Geomorphology,** v.180-181, p. 1-9, 2013. DOI: 10.1016/j.geomorph.2012.08.023

14. CHORLEY, R. J.; SCHUMM, S. A.; SUGDEN, D. E. **Geomorphology**. 1º Ed. New York: Methuen Inc, 1985. 607p.

15. CHRISTOFOLETTI, A. Análise morfométrica de bacias hidrográficas. **Notícia Geomorfológica**, v. 18, n. 9, p. 35-64, 1969.

16. CORRÊA, A. C. B; FONSECA, D. N. Lineamentos de drenagem e de relevo como subsídio para a caracterização morfoestrutural e reativações neotectônicas da área da bacia do rio Preto, Serra do Espinhaço Meridional-MG. **Revista de Geografia**, v. especial, VIII SINAGEO, n. 1, p. 72-86, 2010.

17. COUTO, E. V.; FORTES, E.; FERREIRA, J. H D. Índices geomorfológicos aplicados a análise morfoestrutural da zona de falha do Rio Alonzo – PR. **Revista Brasileira de Geomorfologia,** v. 14, n. 4, p. 287-297, 2013. DOI: doi.org/10.20502/rbg.v14i4.323

18. COX, R. T. Analysis of drainage and basin symmetry as a rapid technique to identify areas of possible Quaternary tilt-block tectonics: an example from the Mississipi Embayment. **GSA Bulletin**, v. 106, n. 5, p. 571-581, 1994. DOI: 10.1130/0016-7606(1994)106<0571:AODBSA>2.3.CO;2

19. CRITELLI, T.; VESPASIANO, G.; APOLLARO, C.; MUTO, F.; MARINI, L; DE ROSA, R. Hydrogeochemical study of an ophiolitic aquifer: a case study of Lago (Southern Italy, Calabria). **Environmental Earth Sciences,** v. 74, p. 533-543, 2015. DOI: 10.1007/s12665-015-4061-z

20. CUTTS, K.; LANA, C.; MOREIRA, H.; ALKMIM, F.; PERES, G. G. Zircon U-Pb and Lu-Hf record from high-grade complexes within the Mantiqueira Complex: First evidence of juvenile crustal input at 2.4–2.2 Ga and implications for the Palaeoproterozoic evolution of the São Francisco Craton. **Precambrian Research,** v. 338, 105567, 2020. DOI: 10.1016/j.precamres.2019.105567

21. DANIELS, J. M. Distinguishing allogenic from autogenic causes of bed elevation change in late Quaternary alluvial stratigraphic records. **Geomorphology,** v. 101, n. 1-2, p. 159-171, 2008. DOI: 10.1016/j.geomorph.2008.05.022

22. DOMINGUES, G. F.; BARBOSA, R. A.; CORRÊA, C. C. S. A.; GUIMARÃES, C. M.; SILEIRA, L. J.; DIAS, H. C. T. Caracterização morfométrica e comportamento hidrológico da bacia hidrográfica do Rio Pardo. **Revista Ifesciências,** v. 6, n. 2, p. 3-16, 2020. DOI: 10.36524/ric.v6i2.502

23. DUNCAN. River behavior. In: BRIERLEY, G. J.; FRYIRS, K. A. **Geomorphology and River Management: Applications of the River Styles Framework**. 1st Ed. Oxford: Blackwell Publishing, 2005. p.143-185. DOI: 10.1002/9780470751367

24. ESRI INC. **ArcMap (versão 10.8)**. Redlands, Estados Unidos, 2020.

25. ETCHEBEHERE, M. L.; SAAD, A. R.; FULFARO, V. C.; PERINOTTO, A. J. Aplicação do Índice "Relação Declividade-Extensão - RDE" na Bacia do Rio do Peixe (SP) para Detecção de Deformações Neotectônicas. **Geol. USP Sér. Cient.**, v. 4, n. 2, p. 43-56, 2004. DOI: 10.5327/S1519-874X2004000200004

26. FONSECA, A. C. L.; NOVO, T. A.; NACHTERGAELE, S.; FONTE-BOA, T. M. R.; VAN RANST, G.; GRAVE, J. D. Differential Phanerozoic evolution of cratonic and non-cratonic lithosphere from a thermochronological perspective: São Francisco Craton and marginal orogens (Brazil). **Gondwana Research,** v. 93, p. 106-126, 2021. DOI: 10.1016/j.gr.2021.01.006

27. GARROTE, J.; COX, R. T.; SWANN, C.; ELLIS, M. Tectonic geomorphology of the southeastern Mississippi Embayment in northern Mississippi, USA. **GSA Bulletin,** v. 118; n. 9-10, p. 1160–1170, 2006. DOI: 10.1130/B25721.1

28. GIMENEZ, V. B.; SALAMUNI, E.; SANTOS, J. M.; PEYERL, W. R. L.; FARIAS, T. F. S.; SANCHES, E. The role of fault reactivation in the geomorphological evolution of coastal landforms on passive continental margins: Evidence from a tectonic estuary in southern Brazil. **Geomorphology,** v. 402, 108132, 2022. DOI: 10.1016/j.geomorph.2022.108132

29. GLOBAL MAPPER. **Global Mapper (versão 23).** 2022. Disponível em: < https://www.bluemarblegeo.com/>. Acesso em: 17 jun. 2022.

30. GOSWAMI, P. K.; PANT, S. Active bidirectional tectonic-tilting in a part of the Almora Klippe, Kumaun Lesser Himalaya, India: Insights from statistical analyses of geomorphic indices. **Quaternary International**, v. 523, p. 46-53, 2019. DOI: 10.1016/j.quaint.2019.06.016

31. GRAVELIUS, H. Grundrifi der gesamten Gewcisserkunde, Band 1: h'lufikunde, **Compendium of Hydrology**, v. 1: Rivers, in German. Goschen, Berlin, Germany, 1914.

32. GURNELL, A. M.; BERTOLDI, W. The impact of plants on fine sediment storage within the active channels of gravel-bed rivers: A preliminary assessment. **Hydrological Processes**, v.36, n.7, e14637, 2022. DOI: doi.org/10.1002/hyp.14637

33. HACK J. T. Stream-profile analysis and stream-gradient index. **J. Res. U.S. Geol. Survey**, v. 1, n. 4, p. 421-429, 1973.

34. HAN, Z.; WU, L.; RAN, Y.; YE, Y. The concealed active tectonics and their characteristics as revealed by drainage density in the North China plain (NCP). **Journal of Asian Earth Sciences,** v. 21, n. 9, p. 989-998, 2003. DOI: 10.1016/S1367-9120(02)00175-X

35. HARE P. W; GARDNER I. W. Geomorphic indicators of vertical neotectonism along converging plate margins. Nicoya Peninsula, Costa Rica. In: XV Annual Binghamton Geomorphology SIMP, 15, 1985, Boston. **Tectonic Geomorphology**… (Procedings) Boston: Allen and Unwin, 1985. p. 123-134.

36. HOBSON, R. D. Surface roughness in topography: quantitative approach. In: CHORLEY, R. J. **Spatial analysis in geomorphology**, 1st Ed. London: Routledge, 1972. p. 1-26. DOI: 10.4324/9780429273346

37. HORTON, R. E. Erosional Development of Streams and Their Drainage Basins: Hydrophysical Approach to Quantitative Morphology. **Geol. Soc. American Bulletin**, v. 56, n. 3, p. 275-370, 1945. DOI: 10.1130/0016-7606(1945)56[275:EDOSAT]2.0.CO;2

38. HUNT, J. D.; FALCHETTA, G.; ZAKERI, B.; NASCIMENTO, A.; SCHNEIDER, P. S.; WEBER, N. A. B.; MESQUITA, A. L. A.; BARBOSA, P. S. F.; JOSÉ DE CASTRO, N. Hydropower impact on the river flow of a humid regional climate. **Climatic Change,** v. 163, p. 379-393, 2020. DOI: 10.1007/s10584-020-02828-w

39. IBGE. **Carta Topográfica de Baiões, Folha SF-23-C-IV-1**. Rio de Janeiro: IBGE, 1969a. Escala 1: 50.000.

40. IBGE. **Carta Topográfica de Formiga, Folha SF-23-C-II-3**. Rio de Janeiro: IBGE, 1969b. Escala 1: 50.000.

41. IBGE. **Carta Topográfica de Arcos, Folha SF-23-C-I-2**. Rio de Janeiro: IBGE, 1970a. Escala 1: 50.000.

42. IBGE. **Carta Topográfica de Pontevila, Folha SF-23-C-III-2**. Rio de Janeiro: IBGE, 1970b. Escala 1: 50.000.

43. KIRBY, E.; WHIPPLE, K. X. Expression of active tectonics in erosional landscapes. **Journal of Structural Geology,** v. 44, p. 44-75, 2012. DOI: 10.1016/j.jsg.2012.07.009

44. KÖPPEN, W. Das geographische System der Klimate. In: KÖPPEN, W.; GEIGER, R. (Ed.). **Handbuch der klimatologie**. Berlin: Gebrüder Bornträger, 1936, p. 1-44.

45. KURIBARA, Y.; TSUNOGAE, T.; SANTOSH, M.; TAKAMURA, Y.; COSTA, A. G.; ROSIÉRE, C. A. Eoarchean to Neoproterozoic crustal evolution of the Mantiqueira and the Juiz de Fora Complexes, SE Brazil: Petrology, geochemistry, zircon U-Pb geochronology and Lu-Hf isotopes. **Precambrian Research,** v. 323, p. 82-101, 2019. DOI: 10.1016/j.precamres.2019.01.008

46. LAVARINI, C.; MAGALHÃES JÚNIOR, A. P. Análise morfométrica de bacias de cabeceira como ferramenta de investigação geomorfológica em média e larga-escala espacial. **Revista Brasileira de Geomorfologia,** v. 14, n. 1, p. 35-46, 2013. DOI: 10.20502/rbg.v14i1.331

47. LAZZARO, M. D.; ZARLENGA, A.; VOLPI. Hydrological effects of within catchment heterogeneity of drainage density. **Advances in Water Resources,** v. 76, p. 157-167, 2015. DOI: 10.1016/j.advwatres.2014.12.011

48. LIMA, J. C. F.; BEZERRA, F. H. R.; ROSSETTI, D. F.; BARBOSA, J. A.; MEDEIRO, W. E.; CASTRO, D. L.; VASCONCELOS, D. L. Neogene–Quaternary fault reactivation influences coastal basin sedimentation and landform in the continental margin of NE Brazil. **Quaternary International**, v. 438, Part A, p. 92-107, 2017. DOI: 10.1016/j.quaint.2016.03.026.

49. LIN, P.; PAN, M.; WOOD, E. F.; YAMAZAKI, D.; ALLEN, G. H. A new vector-based global river network dataset accounting for variable drainage density. **Nature,** v. 8, n. 28, p. 1-9, 2021. DOI: 10.1038/s41597-021-00819-9

50. LOLLO, J. A. **O uso da técnica de avaliação do terreno no processo de elaboração do mapeamento geotécnico: sistematização e aplicação na quadrícula de Campinas.** 1995. Tese (Doutorado em Geotecnia) – Programa de Pós-Graduação em Geotecnia, Escola de Engenharia de São Carlos, Universidade de São Paulo, São Carlos, 1995. 267p.

51. MAKRARI, S.; SHARMA, G.; TALOOR, A. K.; SINGH, M. S.; SARMA, K. K.; AGGARWAL, S. P. Assessment of the geomorphic indices in relation to tectonics along selected sectors of Borpani River Basin, Assam using Cartosat DEM data. **Geosystems and Geoenvironment,** v. 1, n. 1, 100068, 2022. DOI: 10.1016/j.geogeo.2022.100068

52. MANSIKKANIEMI, H. The sinuosity of rivers in northern Finland. **Publicationes Instituti Geographici Universitatis Turkuensis,** v. 52, p. 16-32, 1970

53. MATLAB. **Matlab software (version R2021a).** Natick, Massachusetts: The MathWorks Inc. 2021.

54. MELTON, M. A. **An analysis of the relations among elements of climate, surface properties and geomorphology**. New York: Dept. Geol. Columbia Univ. Tech. Rep., 1957. 102p. DOI: 10.7916/d8-0rmg-j112

55. MILLER, V. C. A Quantitative Geomorphic Study of Drainage Basin Characteristics in the Clinch Mountain Area, Virginia and Tennessee. Department of Geology, Columbia University, Technical Report, n. 3, 1953.

56. MITROFAN, H.; CADICHEANU, N.; NICULAE, L.; CHITEA, F. Hindu Kush intermediate-depth seismicity: A possible explanation for the preferential asymmetry displayed by river catchments within the corresponding epicentral area. **Tectonophysics,** v. 832, 229360, 2022. DOI: 10.1016/j.tecto.2022.229360

57. MONTEIRO, K. A.; TAVARES, B. A. C.; CORRÊA, A. C. Aplicação do índice de Hack no rio Ipojuca para identificação de setores anômalos de drenagem e rupturas de relevo. **Geociências,** v. 33, n. 4, p. 616-628, 2014.

58. MONTGOMERY, D. R.; ABBE, T. B.; BUFFINGTON, J. M.; PETERSON, N. P.; SCHMIDT, K. M.; STOCK, J. D. Distribution of bedrock and alluvial channels in forested mountain drainage basins. **Nature,** v. 381, n. 6583, p. 587-589, 1996. DOI: 10.1038/381587a0

59. MUELLER, E.; PITLICK, J. Sediment supply and channel morphology in mountain river systems: 1. Relative importance of lithology, topography, and climate. **Journal of Geophysical Research: Earth Surface,** v. 118, p. 2325-2342, 2013. DOI: 10.1002/2013JF002843

60. OMIDIJI, J.; STEPHENSON, W.; DICKSON, M.; NORTON, K. Tectonics and shore platform development: Rates and patterns of erosion on recently uplifted mudstone and limestone rocks at Kaikoura Peninsula, New Zealand. **Marine Geology,** v. 451, 106887, 2022. DOI: 10.1016/j.margeo.2022.106887

61. OUCHI, S. Response of alluvial rivers to slow active tectonic movement. **Geological Society of America Bulletin,** v. 96, n. 4, p. 504-515, 1985. DOI: 10.1130/0016-7606(1985)96<504:ROARTS>2.0.CO;2

62. PAIXÃO, R. W.; SALGADO, A. A. R.; FREITAS, M. M. Morfogênese do divisor hidrográfico Paraná/Paraíba do sul: o caso da sub-bacia do Paraíbuna. **Revista Brasileira de Geomorfologia**, v. 20, n. 1, p. 119-136, 2019. DOI: 10.20502/rbg.v20i1.1498

63. PANTA, G.; NASCIMENTO, J. P. H.; MONTEIRO, K. A. Eroded topography in Proterozoic Basement: the case of Capiá river watershed, Semi-arid Northeastern Brazil. **Revista Brasileira de Geomorfologia,** v. 23, n. 4, p. 1929-1946, 2022. DOI: 10.20502/rbg.v23i4.2159

64. PASSARELLA, S.; LADEIRA, S. B. L.; LIESENBERG, V. Morfometria da bacia do Rio São João, MG: uma proposta de entendimento dos limites e da dinâmica das superfícies erosivas. **Revista Brasileira de Geomorfologia,** v. 17, n. 2, p. 241-252, 2016. DOI: 10.20502/rbg.v17i2.790

65. PCI GEOMATICS. **Pci Geomatics Geomatica.** Ontario, Canada. 2016. Disponível em: < https://gogeomatics.ca/subjects/pci-geomatics/>. Acesso em: 18 mai. 2022.

66. PERȘOIU, I.; SIPOS, G.; RĂDOANE, M.; HUTCHINSON, S. M.; MICHCZYŃSKA, D. J.; PERȘOIU, A. Tectonic, climatic and autogenic controls on the Late Quaternary evolution of the Someș fluvial fan, North-East Pannonian Basin, Central Europe. **Geomorphology,** v. 417, 108450, 2022. DOI: 10.1016/j.geomorph.2022.108450

67. PETTS, G. E.; GURNELL, A. M. Hydrogeomorphic Effects of Reservoirs, Dams, and Diversions. In: SHRODER, J. F. (Ed.). **Treatise on Geomorphology**. 2nd Ed. Academic Press, 2022. p. 144-166. DOI: 10.1016/B978-0-12-374739-6.00345-6

68. PHILLIPS, J. D.; LUTZ, J. D. Profile convexities in bedrock and alluvial streams. **Geomorphology,** v. 102, n. 3-4, p. 554-566, 2008. DOI: 10.1016/j.geomorph.2008.05.042

69. PIEDADE, G. C. R. **Evolução de voçorocas em bacias hidrográficas do município de Botucatu, SP**. Tese (Livre Docência) - Faculdade de Ciências Agronômicas, Universidade Estadual Paulista, Botucatu. 1980. 161p.

70. RADAIDEH, O. M. A.; MOSAR, J. Tectonics controls on fluvial landscapes and drainage development in the westernmost part of Switzerland: Insights from DEM-derived geomorphic indices. **Tectonophysics,** v. 768, 228179, 2019. DOI: 10.1016/j.tecto.2019.228179

71. RIBEIRO, J. F.; WALTER, B. M. T. Fitofisionomias do bioma Cerrado In: SANO, S. M.; ALMEIDA, S. P. (Ed.). **Cerrado:** ambiente e flora. 1º Ed. Brasília: Embrapa Cerrados, 1998. p. 87-166.

72. ROCKWARE. **RockWorks Single license: Basic Level (Version 17)** Golden, Colorado, USA. 2016. Disponível em: < https://www.rockware.com/product/rockworks/#>. Acesso em: 18 oct. 2022.

73. ROSSETTI, D. F.; VASCONCELOS, D. L.; BEZERRA, F. H. R.; VALERIANO, M. M.; ALVES, F. C.; MOLINA, E. C. A large-scale domal relief due to intraplate neotectonic compression in central Amazonia. **Geomorphology**, v. 407, 108218, p. 1-20, 2022. DOI: 10.1016/j.geomorph.2022.108218

74. SAMPAIO, T. V. M. **Parâmetros morfométricos para melhoria da acurácia do mapeamento da rede de drenagem – uma proposta baseada na análise da Bacia Hidrográfica do Rio Benevente - ES.** 2008. Tese (Doutorado em Geociências) – Programa de Pós-Graduação em Geociências, Universidade Federal de Minas Gerais, Belo Horizonte. 2008. 147p.

75. SAMPAIO, T. V. M.; AUGUSTIN, C. H. R. R. Índice de concentração da rugosidade: uma nova proposta metodológica para o mapeamento e quantificação da dissecação do relevo como subsídio a cartografia geomorfológica. **Revista Brasileira de Geomorfologia**, v. 15, n. 1, p. 47-60, 2014. DOI: 10.20502/rbg.v15i1.376

76. SANTOS, T. M. B.; TASSINARI, C. C. G.; FONSECA, P. E. Diachronic collision, slab break-off and long-term high thermal flux in the Brasiliano–Pan-African orogeny: Implications for the geodynamic evolution of the Mantiqueira Province. **Precambrian Research,** v. 260, p. 1-22, 2015. DOI: 10.1016/j.precamres.2014.12.018

77. SCHNEIDER, A.; JOST, A.; COULON, C.; SILVESTRE, M.; THÉRY, S.; DUCHARNE, A. Global-scale River network extraction based on high-resolution topography and constrained by lithology, climate, slope, and observed drainage density. **Geophysical Research Letters,** v. 44, p. 2773-2781, 2017. DOI: 10.1002/2016GL071844

78. SCHUMM, S. A. Evolution of drainage systems and slopes in badlands at Perth Amboy, New Jersey. **Geol Soc Am,** v. 67, p. 597-646, 1956. DOI: 10.1130/0016-7606(1956)67[597:eodsas]2.0.co;2

79. SCHUMM, S. A. Sinuosity of alluvial rivers in the great plains. **Geol Soc Am**, Bull 74, n. 9, p.1089–1100, 1963. DOI: 10.1130/0016-7606(1963)74[1089:SOAROT]2.0.CO;2

80. SCHUMM, S. A. Alluvial River response to active tectonics. In: WALLACE, R. E. (Ed.) **Active Tectonics.** 1º Ed. Washington DC: National Academy Press, 1986. p. 80-94.

81. SCHWANGHART, W.; KUHN, N. J. TopoToolbox: A set of MATLAB functions for topographic analysis. **Environmental Modelling & Software,** v. 25, n. 6, p. 770-781, 2010. DOI: 10.1016/j.envsoft.2009.12.002

82. SCHWANGHART, W.; MOLKENTHIN, C.; SCHERLER, D. A systematic approach and software for the analysis of point patterns on river networks. **Earth Surface Processes and Landforms,** v. 46, n. 9, p. 1847-1862, 2021. DOI: 10.1002/esp.5127

83. SCHWANGHART, W.; SCHERLER, D. Short Communication: TopoToolbox 2 – MATLAB-based software for topographic analysis and modeling in Earth surface sciences. **Earth Surface Processes and Landforms,** v. 2, n. 1, p. 1-7, 2014. DOI: 10.5194/esurf-2-1-2014

84. SCHWANGHART, W.; SCHERLER, D. Bumps in river profiles: uncertainty assessment and smoothing using quantile regression techniques. **Earth Surface Processes and Landforms**, v.5, n. 4, p.821-839, 2017. DOI: 10.5194/esurf-5-821-2017

85. SEEBER, L.; GORNITZ, V. River profiles along the Himalayan arc as indicators of active tectonics. **Tectonophysics,** v. 92, n. 4, p. 335-367, 1983. DOI: 10.1016/0040-1951(83)90201-9

86. SILVA, E. C. R.; ALVES, F. B.; SOUZA, M. J. R.; PROGÊNIO, M. F.; COSTA, C. E. A. S. Modelagem Hidrodinâmica como Ferramenta para Gerenciamento de Riscos Hídricos no Rio Tapajós. **Revista Brasileira de Geomorfologia,** v. 22, n. 2, p. 337-350, 2021. DOI: 10.20502/rbg.v22i2.1975

87. SILVA, M. A.; PINTO, C. P.; PINHEIRO, M. A. P.; MARINHO, M. S.; LOMBELLO, J. C.; PINHO, J. M. M. P.; GOULART, L. E. A.; MAGALHÃES, J. R. **Mapa geológico do estado de Minas Gerais**. CPRM, 2020. Escala 1:1.000.000 Available in: <https://rigeo.cprm.gov.br/xmlui/handle/doc/21828?show=full>. Access at: 22 feb. 2023.

88. SMERAGLIA, L.; GIUFFRIDA, A.; GRIMALDI, S.; PULLEN, A.; LA BRUNA, V.; BILLI, A.; AGOSTA, F. Fault-controlled upwelling of low-T hydrothermal fluids tracked by travertines in a fold-and thrust belt, Monte Alpi, southern apennines, Italy. **Journal of Structural Geology,** v. 144, 104276, 2021. DOI: 10.1016/j.jsg.2020.104276

89. SOTCHAVA, V. B. **O estudo de geossistemas.** Instituto de Geografia, USP, São Paulo: Ed. Lunar, 1977. 51p.

90. SOUSA, F. A.; RODRIGUES, S. A. Aspectos morfométricos como subsídio ao estudo da condutividade hidráulica e suscetibilidade erosiva dos solos. **Mercator**, v. 11, n. 25, p. 141-151, 2012. DOI: 10.4215/RM2012.1125.0011

91. SOUZA, C. M. P.; LIMA, C. C. U.; COSTA, L. M.; VELOSO, G. V.; GOMES, R. L.; LEITE, M. E.; FERNANDES-FILHO, E. I. Geomorphic indices, machine learning and osl palynology chronology to assess neotectonic deformation in the continental margin – Northeastern Brazil. **Journal of South American Earth Sciences,** v. 118, 103931, 2022. DOI: 10.1016/j.jsames.2022.103931

92. SOUZA, D. V.; MARTINS, A. A..; FARIA, A. L. L. Aplicação do Índice de Hack (SL) a um trecho do Rio Zêzere, Portugal. **Revista Brasileira de Geomorfologia**, v. 12, n. 1, p. 23-28, 2011. DOI: 10.20502/rbg.v12i1.215

93. STRAHLER, A. N. Hypsometric (area-altitude) analysis of erosion al topography. **Geological Society of America Bulletin**, v. 63, n. 11, p. 1117-1142, 1952. DOI: 10.1130/0016-7606(1952)63[1117:HAAOET]2.0.CO;2

94. SZMAŃDA, J. B.; GIERSZEWSKI, P. J.; HABEL, M.; LUC, M.; WITKOWSKI, K.; BORTNYK, S.; OBODOVSKYI, O. Response of the Dnieper river fluvial system to the river erosion caused by the operation of the Kaniv hydro-electric power plant (Ukraine). **Catena,** v. 202, 105265, 2021. DOI: 10.1016/j.catena.2021.105265

95. THAYER, J. B.; ASHMORE, J. Floodplain morphology, sedimentology, and development processes of a partially alluvial channel. **Geomorphology,** v. 269, p. 160-174, 2016. DOI: 10.1016/j.geomorph.2016.06.040

96. TOONE, J.; RICE, S. P.; PIÉGAY, H. Spatial discontinuity and temporal evolution of channel morphology along a mixed bedrock-alluvial river, upper Drôme River, southeast France: Contingent responses to external and internal controls**.** **Geomorphology,** v. 205, n. 4, p. 5-16, 2014. DOI: 10.1016/j.geomorph.2012.05.033

97. TUCKER, G. E.; CATANI, F.; RINALDO, A.; BRAS, R. L. Statistical analysis of drainage density from digital terrain data. **Geomorphology,** v. 36, n. 3-4, p. 187-202, 2001. DOI: 10.1016/S0169-555X(00)00056-8

98. UFV - Universidade Federal de Viçosa; CETEC - Fundação Centro Tecnológico de Minas Gerais; UFLA - Universidade Federal de Lavras; FEAM - Fundação Estadual do Meio Ambiente. **Mapa de solos do Estado de Minas Gerais**: legenda expandida. Belo Horizonte: Fundação Estadual do Meio Ambiente, 2010. Escala 1:650.000. Available in: < https://dps.ufv.br/softwares/>. Access at: 22 feb. 2023

99. USGS - United States Geological Survey. **Earth Explorer**. Available in: <https://earthexplorer.usgs.gov/> Access at: 22 feb. 2023.

100. VILLELA, S. M.; MATTOS, A. **Hidrologia aplicada**. São Paulo: McGraw-Hill do Brasil, 1975. 245p.

101. WHIPPLE, K. X.; DIBIASE, R. A.; CROSBY, B. T.; JOHNSON, J. P. L. Bedrock Rivers. In: SHRODER, J. F. (Ed.). **Treatise on Geomorphology**. 2nd Ed. Academic Press, 2022. p. 865-903. DOI: DOI: 10.1016/B978-0-12-374739-6.00345-6

WOHL, E. E.; MERRIT, D. M. Bedrock channel morphology. **GSA Bulletin,** v. 113, n. 9, p. 1205-1212, 2001. DOI: 10.1130/0016-7606(2001)113<1205:BCM>2.0.CO;2